THE ASTROPHYSICAL JOURNAL, 417:579–594, 1993 November 10

THE DIFFUSE IONIZED INTERSTELLAR MEDIUM: STRUCTURES RESULTING FROM IONIZATION BY O STARS

WALTER WARREN MILLER III
Department of Astronomy, University of Wisconsin—Madison, 475 North Charter Street, Madison, WI 53706
AND
DONALD P. COX
Department of Physics, University of Wisconsin—Madison, 1150 University Avenue, Madison, WI 53706
Received 1992 December 28; accepted 1993 May 17

ABSTRACT

We have explored the possibility that the diffuse ionized gas of the Galaxy is kept ionized by O stars, and that such gas consists of the dilute portions of O star H II regions in a multiple component interstellar medium. To make this exploration, we calculated the H II region structures for the known Galactic O stars and compared the integral properties of the ensemble (dispersion and emission measures) with the observational data.

Our model assumes a smooth intercloud (or more precisely extracloud) medium whose density depends only on z, and a statistical distribution of small, opaque clouds. The latter have line of sight mean free path $\lambda(z)$ between encounters and are assumed to attenuate the radiation field much as dust grains do, with differential fractional loss dr/λ in path dr on all sight lines, rather than forming distinctions between shadowed and unshadowed lines of sight.

With the simplified assumptions of our standard cloud model, good quantitative agreement is found for the electron density as a function of z and the dispersion measures to pulsars at high and low latitudes as well as quantitative agreement for summary measures such as the mean vertical column density of electrons, the average Hα surface brightness perpendicular to the Galactic plane, and its decrease at high latitude. The implications of our model to the diffuse interstellar medium and to the distribution of Lyman continuum absorbers in the Galaxy are discussed in detail.

We present Aitoff projections of the predicted Hα surface brightness, the corresponding electron column density, and the residual neutral column density over the sky. We also include views of the ionized gas structure in the solar vicinity, an Hα view of the Galaxy from above the plane, and two edge views (with and without dust extinction) of the Galaxy.

Subject headings: diffuse radiation — H II regions — ISM: structure — stars: early-type

1. INTRODUCTION

The diffuse ionized gas in the Galaxy has become the subject of intense observational study in recent years. Although measurements thus far do not completely specify the distribution of this gas, they have established its existence beyond the traditional thin Galactic disk, its large power requirement, and the substantial contribution of its weight to the interstellar pressure (see Cox 1989, 1990). Specifically, pulsar dispersion measures and interstellar emission lines indicate that the H II has a local density and temperature around 0.1 cm^{-3} and 10^4 K, resides in fully ionized regions that occupy more than 20% of the interstellar volume, and has a scale height exceeding 900 pc placing half of the gas outside $|z| = 600$ pc (Reynolds 1992).

Given the quantity and pervasiveness of diffuse ionized gas in the Galaxy, the maintenance of the ionization requires substantial power input; Reynolds (1990a) estimates 9.5×10^{38} ergs kpc^{-2} s^{-1} from the Galactic Hα brightness at moderate to high latitudes. This severely constrains the possible ionization source, leaving only O-star photoionization and the energy of supernovae as viable candidates based on Abbott's (1982) calculation that 66% of the radiative energy input to the interstellar medium comes from O-star ionizing photons (about 2.2×10^{40} ergs kpc^{-2} s^{-1}) while supernovae provide 9.9×10^{38} ergs kpc^{-2} s^{-1} of kinetic energy. Cox (1989) has shown that, although supernova remnants could in principle produce enough diffuse electrons to explain the pulsar dispersion measures, they fall short of providing the Galactic Hα brightness by at least a factor of 7. On the other hand, the consistency of the power requirement, spectrum, and temperature of the diffuse ionized gas with photoionization suggests that O stars are responsible for the widespread ionization.

Indeed, both Mathis (1986) and Bregman & Harrington (1986) concluded that O stars are the likely source of the diffuse ionization from examining photoionization models. In particular, Mathis (1986) compared interstellar shocks with photoionization, showing that the observed uniformity of the line ratio [S II]/Hα (albeit larger in magnitude than in traditional H II regions; but see § 2) restricts shock speeds to an unrealistically narrow range of values. Torres-Peimbert, Lazcano-Araujo, & Peimbert (1974), Thuan (1975), and Lynds (1980) specifically explore O stars as an ionization source and conclude that enough O stars exist outside of dense H II regions (Torres-Peimbert et al. 1974; Lynds 1980), or are capable of ionizing out of the Galaxy (Thuan 1975), to produce significant ionization in a low-density medium.

None of these investigations, however, address a substantial problem that plagues O-star photoionization in the diffuse interstellar medium (DISM): the ionizing photons from O stars must be able to ionize gas far from the region the stars nor-

mally occupy, while evading absorption by significant quantities of neutral gas. For this to be possible, the interstellar medium must be sufficiently transparent to hydrogen-ionizing photons, while also sufficiently dense to accumulate the observed dispersion and emission measures.

Using our best estimate of how the extracloud medium is distributed, a statistical approximation to H I clouds, and the locations and luminosities of all known O stars in the solar neighborhood, we examine whether photoionization by O stars satisfies the pair of constraints listed above. First, however, we provide a brief review of the observed properties of the DISM.

2. OBSERVATIONAL SITUATION

Most of the information gathered so far about the diffuse ionized gas is obtained from pointed observations toward pulsars in the disk of the Galaxy (providing information on the mean line of sight electron density), to pulsars in globular clusters and the Magellanic Clouds (providing upper limits to the extent of the electron distribution), and from faint interstellar emission lines (Hα, [S II], [N II], [O II]; providing emission measures, temperatures, excitation conditions, and gas kinematics). Although not discussed here, other useful data come from Galactic rotation measures, ultraviolet interstellar absorption lines, radio synchrotron studies, and 21 cm studies of the neutral part of the DISM.[1]

Dispersion measures (DM $\equiv \int_0^r n_e\, dl$, where n_e is the electron number density in units of cm^{-3} and r is the pulsar distance in parsecs) to globular cluster pulsars at high Galactic latitudes have recently allowed the determination of the total integrated electron column density through most of the ionized hydrogen (Reynolds 1991). Combined with emission measures (EM $\equiv \int_0^r n_e^2\, dl$) from Galactic Hα observations in the same directions, assumed to derive from the same electron distribution, the indications are that the ionized hydrogen is clumped into regions with local average electron density $\bar{n}_e = 0.08$ cm^{-3} and volume filling fraction $f \geq 0.2$ (Reynolds 1991). The electrons also appear to have a scale height exceeding 900 pc (Reynolds 1990a). Dispersion measures to nearby disk pulsars suggest a volume-averaged midplane electron density $\bar{n}_e = 0.025 \pm 0.005$ cm^{-3} excluding the $\sim$0.015 cm^{-3} contribution from traditional H II regions (Weisberg, Rankin, & Boriakoff 1980; Lyne, Manchester, & Taylor 1985; Lyne 1981; Manchester & Taylor 1981; Vivekanand & Narayan 1982; Harding & Harding 1982). Solar neighborhood measurements further suggest that the mean square electron density at the midplane is $\overline{n_e^2} = 0.007$ cm^{-6} (Reynolds 1991) which together with a mean density of 0.025 cm^{-3} implies a local density of about 0.3 cm^{-3} filling 8% of the volume. These latter values are noted by Reynolds (1991) to be uncertain by a factor of 2.

Observations of forbidden lines place a lower limit on the electron temperature of the diffuse ionized gas of $T_e > 5500$ K (Reynolds 1989a). Correspondingly, with an upper limit to the hydrogen temperature of $T_H < 20{,}000$ K imposed by the line widths of Hα and [S II], both are consistent with the expectation that photoionized gas will have a temperature of 8000 K (Reynolds 1985). However, a recent examination of the potential contribution to the heating by photoelectric ejection off dust grains (Reynolds & Cox 1992) may indicate a higher temperature (10,000 K). Interestingly, this mechanism may also explain the anomalously high [S II]/Hα and [N II]/Hα ratios observed in the diffuse ionized gas. For example, an increase in the heating rate of the DISM by a factor of 2 (the range expected by Reynolds & Cox 1992) results in a temperature change from 7000 K to 9700 K, and an increase of both the [S II]/Hα and [N II]/Hα line ratios by a factor of 2.7. Furthermore, the intensity ratio increases with decreasing gas density. The observed intensity ratios increase with distance from the midplane in NGC 891 (Dettmar & Schulz 1992) consistent with this mechanism and a decreasing density.

Looking at other galaxies for clues to the global properties of diffuse ionized gas has recently begun in earnest. A striking example of widespread diffuse ionized gas is seen in NGC 891 (Rand, Kulkarni, & Hester 1990, 1992; Dettmar 1990; Dettmar & Schulz 1992; Sokolowski & Bland-Hawthorn 1992). Viewed edge-on, NGC 891 has a thick diffuse ionized medium much like that of the Milky Way. The gas extends to kiloparsec distances above the midplane, and at least 10 kpc outward from the galactic center. This massive distribution of ionized gas (twice the H II mass surface density of the Milky Way) appears conspicuously linked to young luminous stars in the disk of NGC 891 (Dettmar 1990), but a causal relationship is not yet firmly established. On the other hand, galaxies such as NGC 4565 and NGC 4631 do not have an extended diffuse ionized medium of the magnitude witnessed in the Milky Way and NGC 891 nor do they appear to be in an active star-forming phase (Rand et al. 1992). Clearly, more galaxies must be sampled before firm conclusions about the diffuse gas morphology and ionization history can be drawn.

3. THE PRESENT APPROACH

We have explored the possibility that the diffuse ionized gas of the Galaxy could be kept ionized by O stars, and that such gas consists of the dilute portions of O star H II regions in a multiple-component interstellar medium. To make this exploration, we have calculated the H II region structures and compared the integral properties of the ensemble (dispersion and emission measures) with the observational data.

In principle, one wishes to calculate the distribution of ionized gas provided by the known O stars (with known locations and luminosities) in the known distribution of interstellar material. Unfortunately, the realistic calculation of radiative transfer of hydrogen-ionizing photons through a cloudy interstellar medium is impossible, given the limited knowledge of cloud configurations and distribution.

As a consequence, we have performed a much simpler calculation in which there is a smooth intercloud (or more precisely extracloud) medium whose density depends only on z, and a statistical distribution of small, opaque clouds. The latter have line-of-sight mean free path $\lambda(z)$ between encounters.

We have assumed that clouds attenuate the radiation field much as dust grains do, with differential fractional loss dr/λ in path dr, rather than considering the details of shadowed and unshadowed lines of sight. This approximation is fairly easily justified for clouds of small angular size because scattering, transport of diffuse ionizing radiation (from recombinations to $n = 1$) from unshadowed regions, and the presence of other stars in the associations will tend to blur the shadow pattern. The loss of diffuse radiation from unshadowed sight lines to regions shadowed by clouds raises the effective recombination rate in the unshadowed gas, causing them to absorb more stellar photons and thus to indirectly experience the attenuation as well.

[1] DISM = WNM + WIM = WNM + DIG = NECM + IECM.

The models are time independent. No consideration is given to the time required for a particular O star to create its Strömgren volume, nor is there compensation for O stars moving at high velocities (runaway O stars) through the interstellar medium. Thuan (1975) discusses these time dependent issues in a general sense.

Overlap of the Strömgren volumes of two or more stars should result in extra ionizing photons that would otherwise go into "reionizing" the overlapped region. These photons increase the combined H II region size beyond the union of isolated cases. Since O stars tend to form in close associations, this might be an important effect. Our models do not account for the excess photons due to this phenomenon and are therefore likely to underestimate the extent of H II regions in the vicinity of O associations.

A host of other problems that are neglected either out of a lack of capability to model them, or their relative unimportance in a simplified model such as ours include stellar winds, superbubbles, local clouds and the photoevaporation thereof, the Local Bubble in which the Sun resides, density concentrations toward spiral arms, and dust. The consequences of neglecting these phenomena are discussed in § 5, whereas dust in clouds is tacitly included given our assumption of opaque clouds. Dust is not included in the diffuse interstellar medium; however, it will not extinct significantly at optical wavelengths (with normal gas-to-dust ratios) given that the total column of diffuse gas straight out of the disk is 55 cm^{-3} pc in our models, equivalent to a 55 pc path at 1 cm^{-3}. In the EUV, this path length does not cause significant photon loss either, with slightly more effect along lateral photon paths (that do not reach large distances from the plane anyway due to the clouds).

4. MODEL IMPLEMENTATION

4.1. *Computational Methods*

4.1.1. *Input*

The machine-readable version of the catalog of O-type stars (Garmany, Conti, & Chiosi 1982) was used as the source of spectral type, luminosity class, Galactic location, and bolometric magnitude of all known O stars, and is said to be complete within 2.5 kpc of the Sun. Although this catalog probably misses some stars that are deeply embedded within their own circumstellar material (and, hence, uninteresting to this study), it is probably complete in stars capable of producing large regions of ionization. As used in this investigation, the catalog contained 761 O stars distributed throughout the solar neighborhood and beyond.

Estimates of the Lyman-continuum photon flux for each star were taken from the early-type stellar parameters of Panagia (1973) based on the bolometric magnitude reported in the O-star catalog. Panagia (1973) used model atmospheres that did not include NLTE effects considered in more recent treatments such as those of Kurucz (1979); however, to remain consistent with previous calculations of O-star Strömgren spheres, we have used the earlier results. As consolation, Panagia (1973) notes that his flux estimates are likely to be slightly smaller than those of NLTE, blanketed models. This makes it more difficult for the stars in our models to ionize lengthy paths through the interstellar medium. It should also be noted that we have compressed the photon flux data across luminosity class by normalizing the flux with the appropriate luminosity as given by Panagia (1973). This allows the storage of a single number for each spectral type (Table 1) in terms of the logarithm of the ratio of the number of ionizing photons per second to the luminosity in solar units. Individual stellar photon fluxes are recovered through multiplication by the luminosity of the star computed from the bolometric magnitude.

TABLE 1

IONIZING PHOTON FLUX

Spectral Type	log (N/L) (photons s^{-1} $L_{\odot}^{-1}$)
O3	43.8500
O4	43.8125
O5	43.7825
O5.5	43.7600
O6	43.7000
O6.5	43.6575
O7	43.6225
O7.5	43.5745
O8	43.5400
O8.5	43.4775
O9	43.4100
O9.5	43.2475

4.1.2. *Strömgren Volumes in a Cloudy Interstellar Medium*

The Strömgren volume of each star is calculated by assuming a balance exists between the ionization and recombination rates in the differential solid angle $d\Omega$. Modifications to the calculation of the Strömgren radius, R, within which the extracloud gas is ionized include both attenuation of the radiation by the clouds and the density variation along the line of sight. The number of ionizations per second in $d\Omega$ out to the ionization edge R (if it is bounded at all) is simply $\mathscr{L}_* d\Omega/4\pi$, where $\mathscr{L}_*$ is the total number of ionizing photons emitted per second at the star. The number of recombinations of extracloud gas per second within this same volume V for a pure hydrogen gas is given by

$$\int_0^R \alpha n_e n_p \, dV = \int_0^R \alpha n_e n_p r^2 \, dr \, d\Omega \,, \tag{1}$$

where n_e and n_p are the electron and proton number densities (in units of cm^{-3}), respectively; α is the recombination coefficient for hydrogen; and the r coordinate extends radially outward from the star. Recombinations to the ground state of hydrogen can be ignored since they result in local ionizing photons that are reabsorbed very close to their point of origination (the *on-the-spot* approximation). Furthermore, inside the ionized volume $(r < R)$ $n_e = n_p \approx n_{\rm H}$.

In the absence of clouds, we can write the criterion for R as

$$\mathscr{L}_* \frac{d\Omega}{4\pi} = \alpha \, d\Omega \int_0^R n_{\rm H}^2 r^2 \, dr \,. \tag{2}$$

For a line of sight inclined at angle b above the Galactic plane, the altitude of a point on the line is $z = z_* + r \sin b$, where z_* is that of the star. Because $n_{\rm H}$ depends on z, it is convenient to rewrite equation (2) as

$$\sin^3 b = \frac{4\pi\alpha}{\mathscr{L}_*} \int_{z_*}^{Z} n_{\rm H}^2(z)(z - z_*)^2 \, dz \,, \tag{3}$$

where $R = (Z - z_*)/\sin b$. The geometry of this situation is clarified in Figure 1.

When clouds are included, the derivation is only slightly more complicated. If we introduce $\mathscr{L}(r)$ as the residual photon

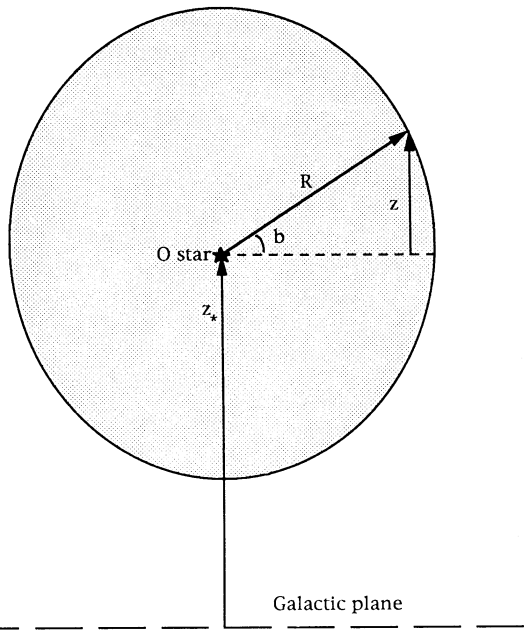

FIG. 1.—The geometry associated with the calculation of the Strömgren volumes. The z-coordinate runs perpendicular to the Galactic plane; z_* denotes the perpendicular height of the star off the midplane; R extends from the star to the ionization edge; b is the angle formed between R and the Galactic plane.

luminosity reaching r, then

$$\frac{d}{dr}\left(\frac{\mathscr{L}\,d\Omega}{4\pi}\right) = -\left(\frac{\mathscr{L}\,d\Omega}{4\pi}\right)\frac{1}{\lambda(r)} - \alpha n_{\rm H}^2 r^2\,d\Omega \tag{4}$$

showing the attenuation due to clouds as well as ionization losses in the extracloud medium. In integral form we have

$$\mathscr{L}(r) = e^{-\tau(r)}\left[\mathscr{L}_* - 4\pi\alpha\int_0^r e^{\tau(r')} n_{\rm H}^2(r')^2\,dr'\right] \tag{5}$$

with $\tau(r) = \int_0^r dr'/\lambda(r')$. The edge of the ionized region is reached at $\mathscr{L}(R) = 0$, where

$$\mathscr{L}_* = 4\pi\alpha\int_0^R e^{\tau(r)} n_{\rm H}^2(r) r^2\,dr\ , \tag{6}$$

or in terms of z,

$$\sin^3 b = \frac{4\pi\alpha}{\mathscr{L}_*}\int_{z_*}^{z} e^{[\tau(z)-\tau(z_*)]/\sin b} n_{\rm ECM}^2(z)(z - z_*)^2\,dz\ . \tag{7}$$

The density appearing in equation (7) is denoted $n_{\rm ECM}$ to emphasize that it consists only of the extracloud medium components.

Because of the density gradient, the Strömgren volume is not spherical, but the above equations can be easily solved in the special direction $b = 0$, to find the radius R at height z_*. In that case, $\tau = r/\lambda(z_*)$, $n_{\rm H} = n_{\rm H}(z_*)$, and

$$\mathscr{L}_* = 4\pi\alpha n_{\rm H}^2\lambda^3\int_0^{R/\lambda} x^2 e^x\,dx\ . \tag{8}$$

Defining the cloud-free radius R_0 as

$$\mathscr{L}_* = \tfrac{4}{3}\pi R_0^3\,\alpha n_{\rm H}^2\ , \tag{9}$$

we have

$$R_0^3 = 3\lambda^3\left\{\left[\left(\frac{R}{\lambda}\right)^2 - 2\left(\frac{R}{\lambda}\right) + 2\right]e^{R/\lambda} - 2\right\}\ . \tag{10}$$

As expected, the Strömgren radii are unchanged for $R \ll \lambda$, but $R/\lambda = 1$, 2, and 3 require $R_0/\lambda = 1.29$, 3.37, and 6.66 or normalized luminosities of $(R_0/\lambda)^3 = 2.15$, 38.3, and 295 rather than the cloud free values of 1, 8, and 27. The result is that very powerful H II regions are strongly limited by the clouds in how far their ionization can extend parallel to the Galactic plane.

This trapping of the ionizing radiation by the clouds is much less severe for directions out of the Galactic plane, however. The radiation which succeeds in traversing the cloud layer suffers no further interference. For a powerful H II region with the vertical R much greater than the cloud scale height, we can approximately factor $e^{\tau(\infty)}$ out of the integral in equation (6), where $\tau(\infty)$ is the optical depth due to cloud blockage from z_* to well outside the Galaxy. The effect is simply to reduce $\mathscr{L}_*$ by $e^{\tau(\infty)}$, roughly a factor of 2 at most. Curiously, however, because of the decreasing $n_{\rm H}$ with increasing height, even a factor of 2 attenuation can have a fairly strong effect on the high z extent of the H II region.

The model extracloud medium (both the WIM and the WNM) are described by two exponentials in $|z|$ specifying the neutral component (the Lockman layer) and the ionized component (the Reynolds layer) with midplane mean densities $\bar{n}_{\rm H\,I} \approx 0.1$ cm^{-3} and $\bar{n}_e \approx 0.025$ cm^{-3}, and scale heights 300 pc and 900 pc, respectively.

The parameters defining the statistical clouds are formulated in terms of a distribution of mean free paths as follows:

$$\tau(z) = \int_0^z \sigma_c(z) n_c(z) dz = \int_0^z \frac{dz}{\lambda(z)} \quad \text{for} \quad z > 0 \tag{11}$$

$$\tau(z) = -\tau(-z) \quad \text{for} \quad z < 0 \tag{12}$$

with

$$\frac{1}{\lambda(z)} = \frac{1}{\lambda(z=0)}\,e^{-1/2(z/z_c)^2}\ . \tag{13}$$

The cloud mean free path at the Galactic midplane, $\lambda(z = 0)$, and the cloud scale height, z_c, are free parameters with values 160 and 100 pc in our standard case. Our choice for the form of $\lambda(z)$ in the standard model is discussed further in §§ 4.2.2 and 5.

Examples of H II regions are illustrated in Figure 2 for our standard parameters. The boundaries of the ionized volumes are shown with and without clouds for a range of main-sequence O-star spectral types at $z_* = 0$ and 50 pc. Except for the brightest stars, the presence of the clouds shrinks the H II regions by about the same factor as a one-unit increase in the spectral subclass.

In our models, we have chosen to record the collective Strömgren volumes as a set of circular cross sections localized in planes parallel to the Galactic plane at equally spaced values of z as illustrated in Figure 3. The vertical spacing between planes was selected to provide good resolution of the H II regions while maintaining reasonable data size. The models are truncated at $|z| = 2.5$ kpc.

4.1.3. *Output*

Once the Strömgren volumes are calculated, Aitoff maps of the sky (as seen from the Sun) for the emission measure, the dispersion measure, and the residual neutral extracloud hydrogen column density, $N_{\rm H\,I} = \int_0^r n_{\rm H\,I}\,dl$, resulting from the H II regions are constructed. The maps are produced by integrating the contributions to n_e, n_e^2, and $n_{\rm H\,I}$ from the H II regions (or the space in between them in the case of $N_{\rm H\,I}$) along each line of sight directed outward from the Sun to the limit of the model. Sight lines with $|b| < 10°$ are ignored because of the increasing

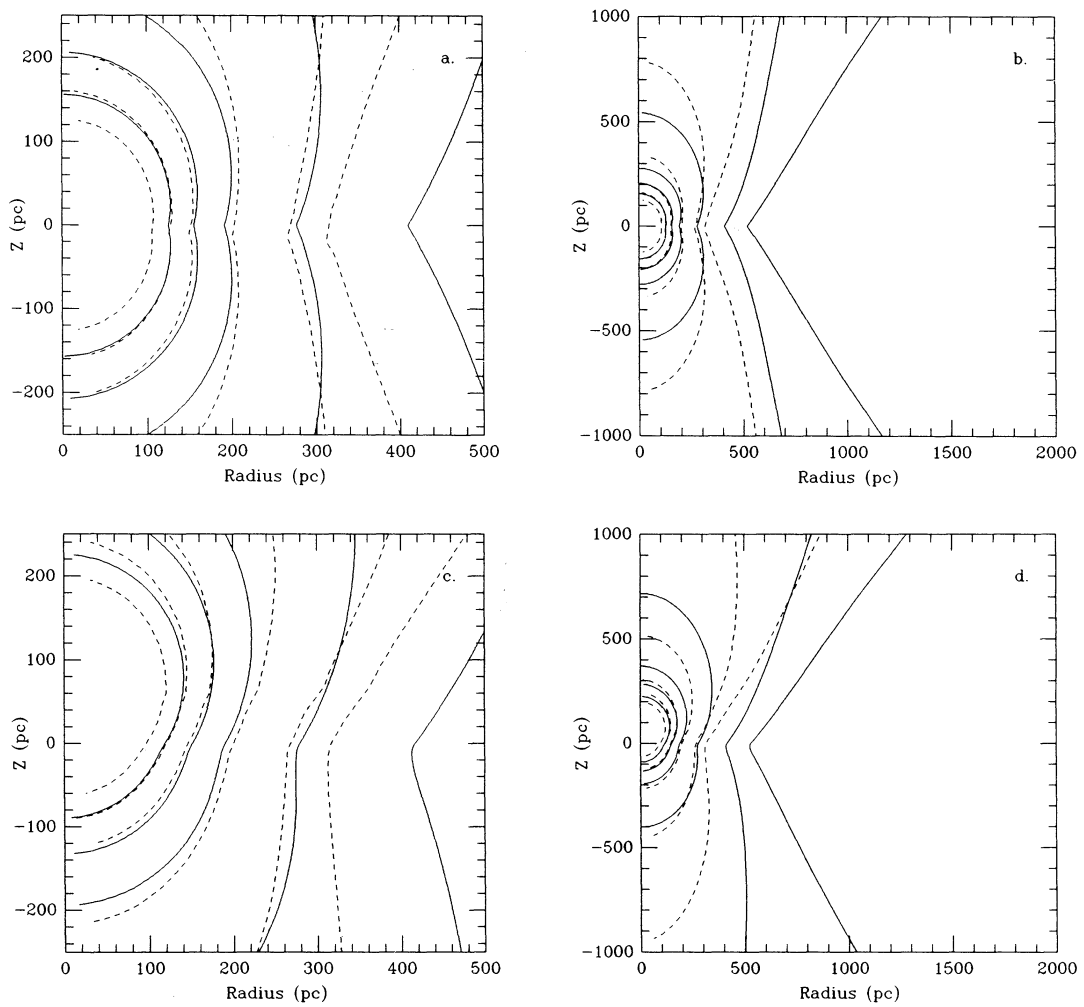

FIG. 2.—(*a*) Half-slices of the H II regions of main-sequence O star spectral types O9 (*innermost solid and dashed curves*), O8, O7, O6, O5, and O4 (*outermost solid and dashed curves*; the solid curve for spectral type O4 is off the scale in Figs. 2*a* and 2*c*) for the cloud-free model (*solid lines*) and for the standard cloud model (*dashed lines*) with the stars located at $z = 0$. (*b*) Same as *a*, but with a larger scale. (*c*) Same as *a*, but with the stars offset from the midplane to $z = +50$ pc. (*d*) Same as *c*, but with a larger scale.

distance traversed between the cross sectional layers used to approximate the Strömgren volumes and the incompleteness of the stellar catalog for distances beyond 2.5 kpc. Ionization within the H II regions is assumed complete so that $n_e = n_{\rm ECM}$ inside and $n_e = 0$ outside.

As shown in Figure 2, the clouds capture a significant fraction of the ionizing photons. Thus, the recombination radiation emitted by their ionized surfaces cannot be neglected in calculating the integrated emission measure. Owing to their large density ($n/n_{\rm ECM} \geq 10^2$), however, their contribution to the dispersion measure can safely be ignored.

To compute the effective square electron density due to the ionized cloud faces, we note that the cloud fluorescence per unit volume is $\mathscr{L}(r)/4\pi r^2\lambda$. So, an effective square electron density from the clouds can be written as

$$n^2_{e,\,\rm cloud} = \frac{\mathscr{L}(r)}{4\pi\alpha r^2\lambda}\,. \tag{14}$$

Substituting equation (5) for $\mathscr{L}(r)$ in equation (14) leads to

$$n^2_{e,\,\rm cloud} = \frac{1}{r^2\lambda(r)e^{\tau(r)}}\left[\frac{\mathscr{L}_*}{4\pi\alpha} - \int_0^r e^{\tau(r')}n_e^2(r')r'^2\,dr'\right]. \tag{15}$$

The total emission measure can now be written

$$\mathrm{EM} = \int_0^r (n^2_{e,\,\rm ECM} + n^2_{e,\,\rm cloud})dl \tag{16}$$

and calculated for each segment of the line of sight r within an H II region. An example of the differences between the total

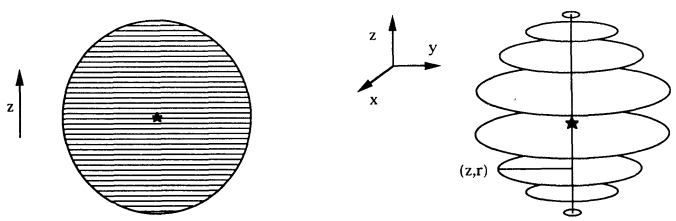

FIG. 3.—A representation of how the Strömgren volume of a star is approximated in our models as a set of circular cross sections. The cross sections formed by equally spaced planes parallel to the Galactic plane serve as the H II volume data in our models.

and extracloud values of EM will be discussed in conjunction with Figure 15.

A useful extraction from the maps is the z-component of both the dispersion and emission measures averaged over Galactic longitude at all galactic latitudes greater than $\pm 10°$. These quantities, labeled $\langle \mathrm{EM} \sin |b| \rangle$ and $\langle \mathrm{DM} \sin |b| \rangle$, are presented with the observations in later sections. Several pulsars have well-determined distances as well as dispersion measures. For these directions, we have calculated the DM in our model out to the distance of the pulsar for direct comparison.

Model values of $\bar{n}_e$ and $\overline{n_e^2}$ as functions of z have also been calculated for gas inside columns of different radii centered on the Sun. This is achieved by evaluating the fraction of ionized to total volume within the column for each z at which Strömgren cross sections are stored, and multiplying by n_{ECM} or n_{ECM}^2, respectively.

4.2. *Model Parameters and Results*

4.2.1. *Cloud-free Model*

With the cloud-free model we attempt to verify that known O stars in the solar neighborhood can produce sufficient ionization to account for the DISM without the attenuating effect of clouds. If this were not possible, then O stars could not be considered viable candidates for the ionization source. Using equation (3), the Strömgren volumes were calculated in a cloud-free medium.

Figure 4 shows the resulting mean (for cylinder radius 1 kpc) electron density as a function of z for this case. The large midplane electron density ($\langle n_e \rangle_0 = 0.095$ cm^{-3}) and the complete ionization of the extracloud medium above $|z| \approx 500$ pc demonstrate an overabundance of ionizing photons. In Figures 5 and 6, $\langle \mathrm{DM} \sin |b| \rangle$ and $\langle \mathrm{EM} \sin |b| \rangle$ versus Galactic latitude are plotted. Both sets of model data, not surprisingly, exceed the average cosecant dependence demonstrated by the observations (*dashed lines*).

4.2.2. *Standard Cloud Model*

We chose as initial values for the statistical cloud parameters those of the standard H I clouds described by Spitzer (1978).

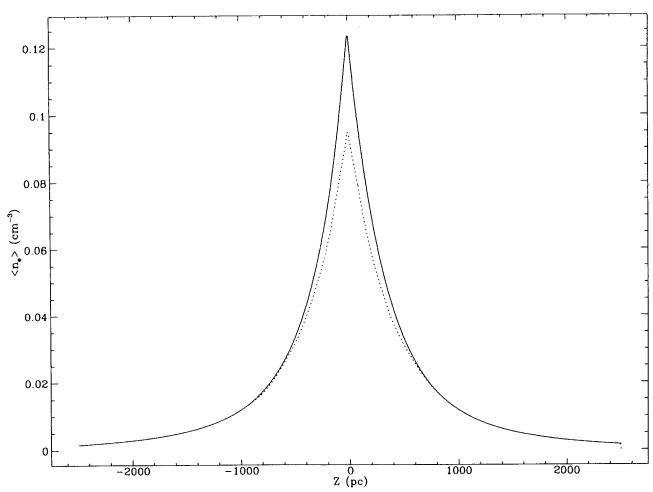

FIG. 4.—The mean electron density plotted against distance z from the Galactic plane (*dotted curve*) inside a cylinder of radius 1000 pc for the cloud-free model. The solid curve is the total extracloud hydrogen density profile used in the model (i.e., the difference between the solid and dotted curves is the diffuse neutral hydrogen density).

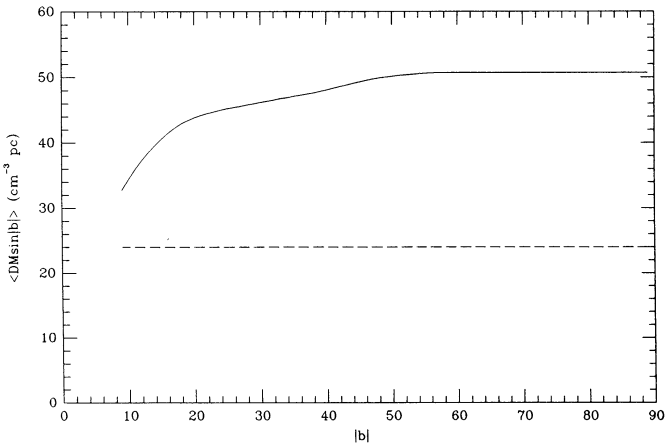

FIG. 5.—The component of the dispersion measure perpendicular to the Galactic plane averaged over Galactic longitude vs. $|b|$ for $|b| > 10°$, for the cloud-free model (*solid curve*). The dashed line is the average observed dispersion measure.

The clouds have a scale height $z_c = 100$ pc, and at the Galactic midplane a mean free path between encounters $\lambda(z = 0) = 160$ pc (i.e., on average there are l/λ clouds on a path of length l). Because the clouds in our models are supposed to represent the Galactic behavior of interstellar clouds, and less so their attributes on small scales, we were less concerned about finding precise cloud parameters than we were about verifying that the model results do not fluctuate wildly over a wide range of cloud parameters.

To this end, we ran a grid of models using a range of cloud mean free paths λ and extracloud medium midplane densities n_{H} (these variables affect quantities at the midplane more than do the cloud or the extracloud medium scale heights) and tabulated the resulting midplane mean electron densities, $\langle n_e \rangle_0$, due to the O stars. We found that $\langle n_e \rangle_0$ varied by less than a factor of 1.5 over a range of λ from 120 to 240 pc, and a range of n_{H} from 0.1 to 0.15 cm^{-3}. We take this to imply that our standard case represents all nearby parameter space fairly well. It is possible that a variation of all of the free parameters in our model in concert might yield a set that fit the data better than our standard case, but real improvement requires a better understanding of what clouds are like in the interstellar

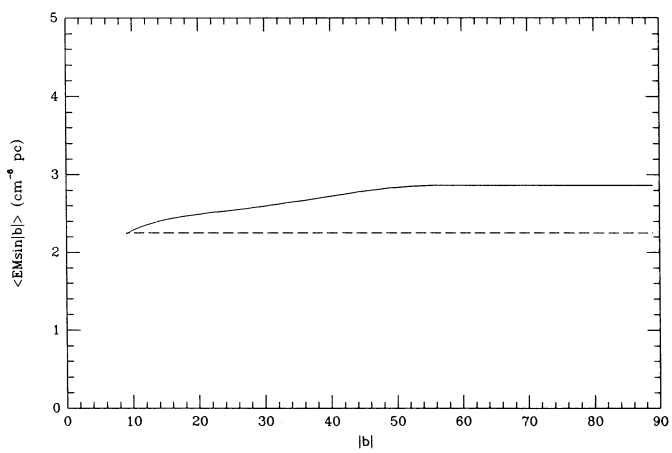

FIG. 6.—The component of the emission measure perpendicular to the Galactic plane averaged over Galactic longitude vs. $|b|$ for $|b| > 10°$, for the cloud-free model (*solid curve*). The dashed line is the average observed emission measure.

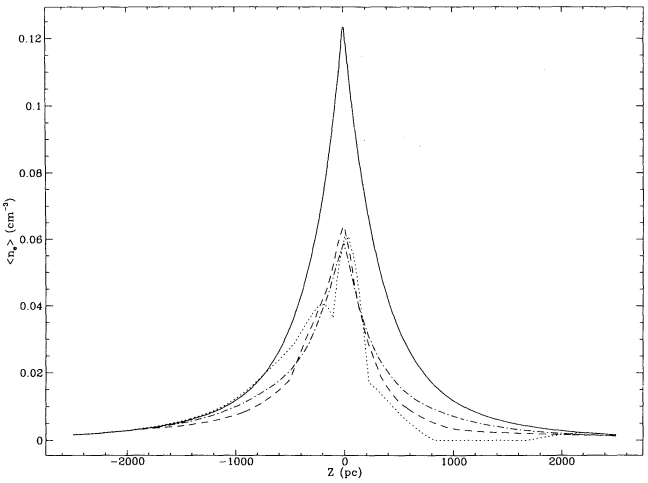

FIG. 7.—The mean electron density plotted against the distance z from the Galactic plane for the standard cloud model calculated within a column centered about the Sun of radius 200 pc (*dotted curve*), 1000 pc (*dashed curve*), and 2500 pc (*dot-dashed curve*). The solid curve is the total extracloud hydrogen density profile used in the model (i.e., the difference between the solid and dotted curves is the diffuse neutral hydrogen density).

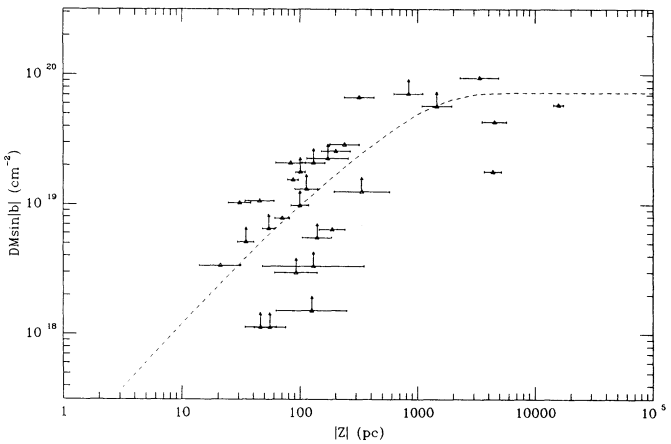

FIG. 9.—For the standard cloud model, the component of the dispersion measure perpendicular to the Galactic plane plotted against the distance z from the Galactic plane for the same directions and distances as the pulsars in Fig. 10. Horizontal lines span the uncertainty in z for the pulsars. Lower limits indicate those directions and distances that sampled space beyond the completeness range of our models. The dashed line is computed from a total electron density distribution estimated from the pulsar observations [$n_e(z) = 0.025e^{-z/900} + 0.015e^{-z/70}$ cm^{-3} for z in parsecs; Reynolds 1990a].

medium and a model that accounts for those details. A thorough discussion of the distribution (both in the Galaxy and in column density) of cold H I clouds inferred from 21 cm observations, and how those observations bear on our model results appears in § 5. With this in mind, we present only the results of our standard cloud model below.

Figure 7 shows the mean electron density versus z for three choices of the column radius inside which the average is calculated. The radii are 200, 1000, and 2500 pc; the largest averages over the entire region for which the O-star catalog is reported complete. The mean square electron density (no ionized cloud surface contribution) versus z for a 1000 pc column radius appears in Figure 8. The mean and mean square electron densities at the midplane are 0.06 cm^{-3} and 0.008 cm^{-6}, respectively.

In Figure 9, the component of the dispersion measure perpendicular to the Galactic plane (DM sin $|b|$) is plotted against z for the directions and distances to the pulsars in the corresponding plot of Reynolds (1989b; reproduced in Fig. 10). The dashed line in both figures derives from an estimate of the total electron density distribution formed from the pulsar dispersion measure data [$n_e(z) = 0.025e^{-z/900} + 0.015e^{-z/70}$ cm^{-3} for z in parsecs; Reynolds 1990a]. Horizontal error bars denote the uncertainty in the z of each pulsar, and data points indicated as lower limits in Figure 9 are sight lines that exceed the O-star catalog completeness limit while still in the disk of the Galaxy. These sight lines potentially underestimate the electron column density due to undiscovered O stars outside the catalog completeness limit. Figure 11 shows a point by point comparison of the (DM sin $|b|$) from our model and from Reynolds (1989b) for those data points in Figure 9 that are not lower limits. The solid line has a slope of 1, and the dashed lines delineate a factor of 2 difference.

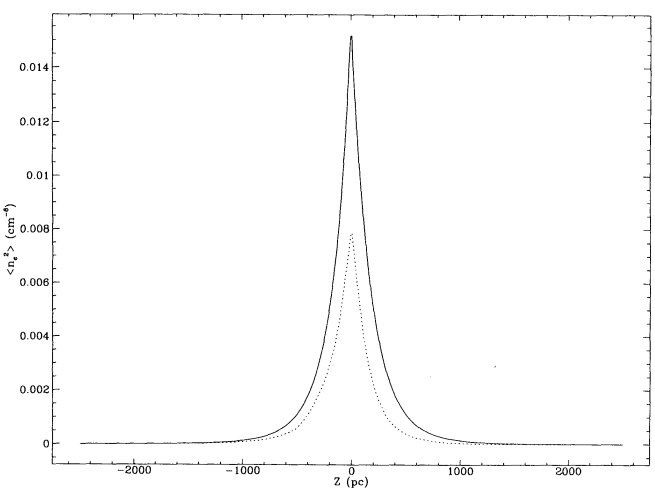

FIG. 8.—The mean square electron density plotted against the distance z from the Galactic plane inside a cylinder of radius 1000 pc for the standard cloud model (*dotted curve*). The solid curve is the square of the total extracloud hydrogen density profile used in the model.

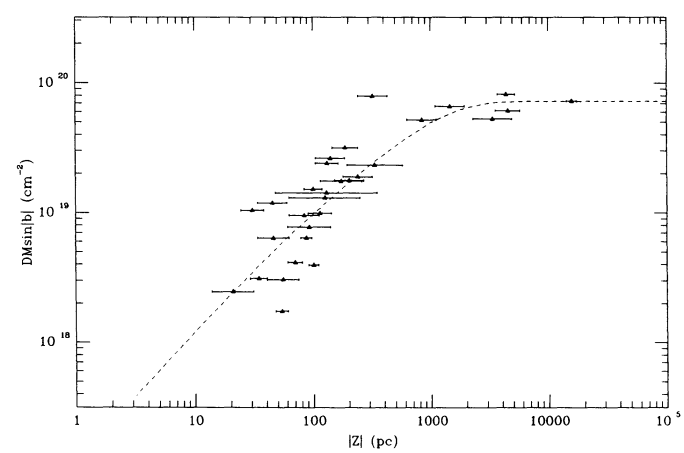

FIG. 10.—The component of the dispersion measure perpendicular to the Galactic plane plotted against the distance z from the Galactic plane for the pulsars in Reynolds (1989b). Horizontal lines span the uncertainty in z for the pulsars. The dashed line is the same electron density distribution as in Fig. 9.

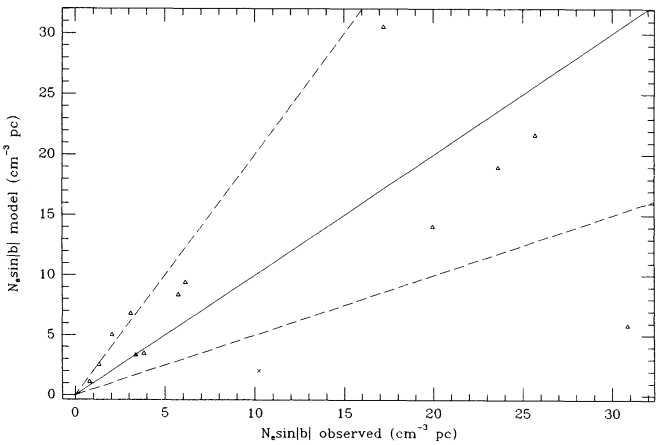

FIG. 11.—A direct comparison of the component of the electron column density (i.e., dispersion measure) perpendicular to the Galactic plane from the standard cloud model (for those sight lines in Fig. 9 not indicated as lower limits) with the observed values in Reynolds (1989b). The solid line has a slope of 1; the dashed lines delineate a factor of 2 difference. PSR 0823+26 (discussed in the text) is shown as a cross.

Aitoff projections from our standard cloud model of the emission measure (including ionized cloud faces), dispersion measure, the vertical component of the dispersion measure (DM sin $|b|$), and the residual neutral hydrogen column density are shown in Figure 12 (Plate 26). Figure 13 presents three views of our model in emission measure (including the cloud brightness correction), the first a face-on view of a 10 kpc square region centered on the Sun, the second and third as if our Galaxy were viewed edge-on encompassing the same volume as in the face-on image, with and without corrections for interstellar extinction. (Recall the catalogue incompleteness beyond 2.5 kpc.) The longitudinally averaged quantities $\langle$DM sin $|b|\rangle$ and $\langle$EM sin $|b|\rangle$ are plotted against Galactic latitude in Figures 14 and 15. Additionally, Figure 15 contains both the total $\langle$EM sin $|b|\rangle$ (including ionized cloud faces) and the contribution from the extracloud medium alone. Finally, Figure 16 shows various slices through the three-dimensional data set in the vicinity of the Sun (Tables 2 and 3 index star names in Figs. 16*a* and 16*f*, respectively).

5. DISCUSSION

Clearly, the known O stars in the solar neighborhood can ionize to great extent a diffuse extracloud medium like that in the cloud-free model. Earlier predictions that the available O-star power meets (and largely exceeds) the power requirement of the DISM based on O-star ionizing photon fluxes and the Hα emission from the DISM are borne out. For example, in Figure 4 the mean electron density at the midplane is much higher ($\langle n_e \rangle_0 = 0.095$ cm^{-3}) than the typical value obtained from dispersion measures to pulsars ($\bar{n}_e \approx 0.03$ cm^{-3}) suggesting an overionization of the plane. At high z, the diffuse gas becomes completely ionized beyond $|z| \approx 500$ pc. Consequently, the longitudinally averaged vertical components of the dispersion measure (Fig. 5) and emission measure (Fig. 6) surpass their respective observational values (*dashed lines*). (The decrease of the model $\langle$DM sin $|b|\rangle$ and $\langle$EM sin $|b|\rangle$ at low latitudes in the figures is due to stellar catalog incompleteness for distances greater than 2.5 kpc). The ensemble of H II regions formed in strictly an extracloud medium exceeds the ionization seen in the DISM. If O stars are the source of the DISM ionization, additional sinks of ionizing photons are present in the plane that reduce the filling factor of H II there, yet do not significantly inhibit the escape of ionizing radiation to high z.

The remainder of this discussion, therefore, focuses on our standard cloud case, specifically exploring to what degree it reproduces the high-z ionization (as in the cloud-free case) and a reasonable mean electron density at the midplane (unlike the cloud-free model). We begin this examination with the computed mean and mean square electron densities as a function of z.

Figure 7 contains three separate determinations of $\bar{n}_e(z)$ within different sized columns of gas centered on the Sun. The dotted curve is for a column radius of 200 pc, thus sampling only very local gas. As might be expected, this calculation shows the most variation as a function of z. Note particularly the asymmetry with respect to $\pm z$; there is a clear deficit of H II on the $+z$ side of the disk (an observed fact; see Reynolds 1984), whereas complete ionization occurs for $z \leq -600$ pc. A more uniform variation of $\bar{n}_e(z)$ is seen for larger column radii (the dashed curve is for a 1 kpc radius; the dot-dashed curve is

TABLE 2

INDEX TO STARS IN FIGURE 16*a*

Index	Star Name	Index	Star Name
4	HD 164794	318	S2411
15	HD 160641	328	HD 256725
25	HD 157857	340	HD 265134
36	HD 168076	341	HD 60848
49	BD −124979	379	HD 61347
50	HD 167971	427	CPD −352212
54	HD 168112	429	CPD −382036
59	HD 166734	452	HD 298429
62	BD −114620	468	HD 92504
66	BD −104682	473	HD 91651
68	HD 169582	502	HD 93249
93	BD +293772	503	HD 93128
94	HD 186980	504	HD 93129B
99	HD 190864	506	CPD −582620
101	HD 190429	508	CPD −592603
112	HD 193682	511	CPD −592600
114	HD 228766	513	HD 93027
123	HD 193514	520	HD 93222
124	HD 192281	534	CPD −582908
128	HD 229232	545	HD 96670
129	HD 189957	558	HD 97166
142	HD 229196	562	HD 95992
143	BD +41368	599	HD 104649
148	BD +404220	611	CPD −613230
150	CYGOB 222	613	HD 109978
151	CYGOB 29	616	CPD −604312
152	BD +404227	627	CPD −613549
154	CYGOB 28C	638	HD 120678
155	CYGOB 28B	649	HD 124979
157	CYGOB 27	657	HD 156359
162	BD +413807	661	HD 147331
163	HD 188209	671	HD 148937
164	HD 191781	675	HD 150197
183	HD 206327	684	HD 151018
188	HD 210839	699	HD 152147
191	HD 215835	707	HD 326331
223	HD 108	709	HD 152248
261	HD 15558	712	HD 152314
264	HD 15629	716	HD 152333
265	HD 15570	728	HD 150475
273	HD 17505	733	HD 156172
289	HD 30614	744	HD 156134
291	BD +56864	754	HD 159176
302	BD +391328	576	HD 156351

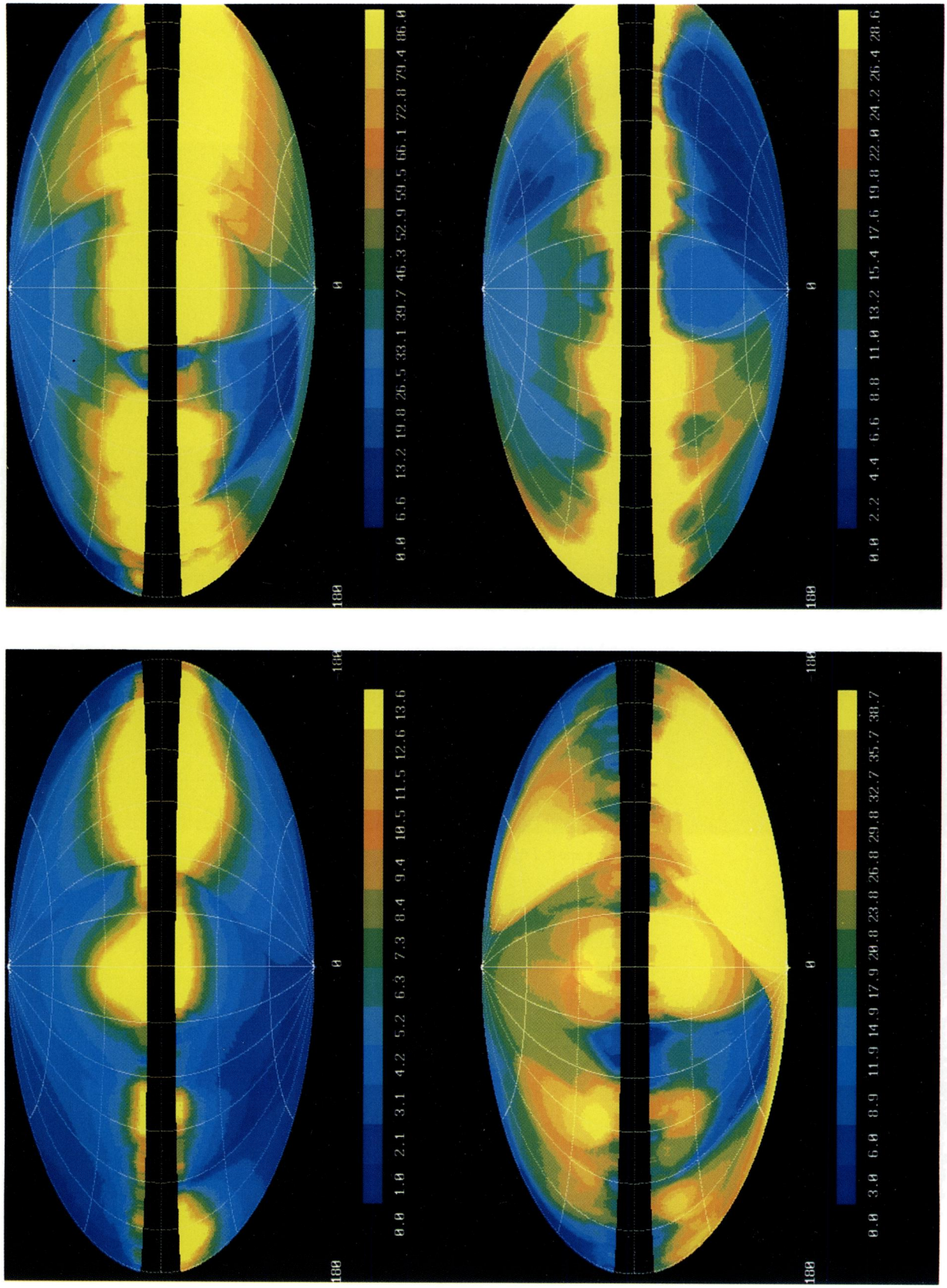

FIG. 12.—Aitoff projections from our standard cloud model of the (*upper left*) the emission measure (including ionized cloud faces), (*upper right*) the dispersion measure, (*lower left*) the vertical component of the dispersion measure (DM sin $|b|$), and (*lower right*) the residual neutral hydrogen column density. The projections are in Galactic coordinates (l, b) centered on $l = 0$ at 1° resolution. The scales are in units of cm^{-6} pc, cm^{-3} pc, cm^{-3} pc, and $\text{cm}^{-2} \times 10^{19}$, respectively. The quantities associated with each color bin represent upper limits to the bin of that color with the exception of the first bin (0.0 means truly 0.0) and the last bin (this bin contains everything greater than or equal to the bin label).

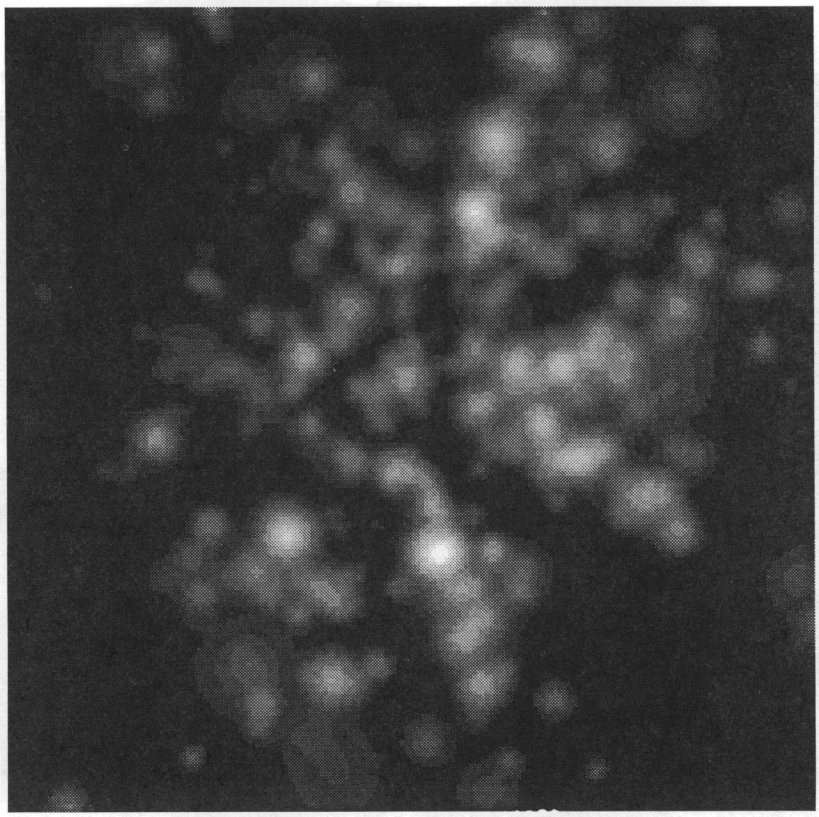

FIG. 13*a*

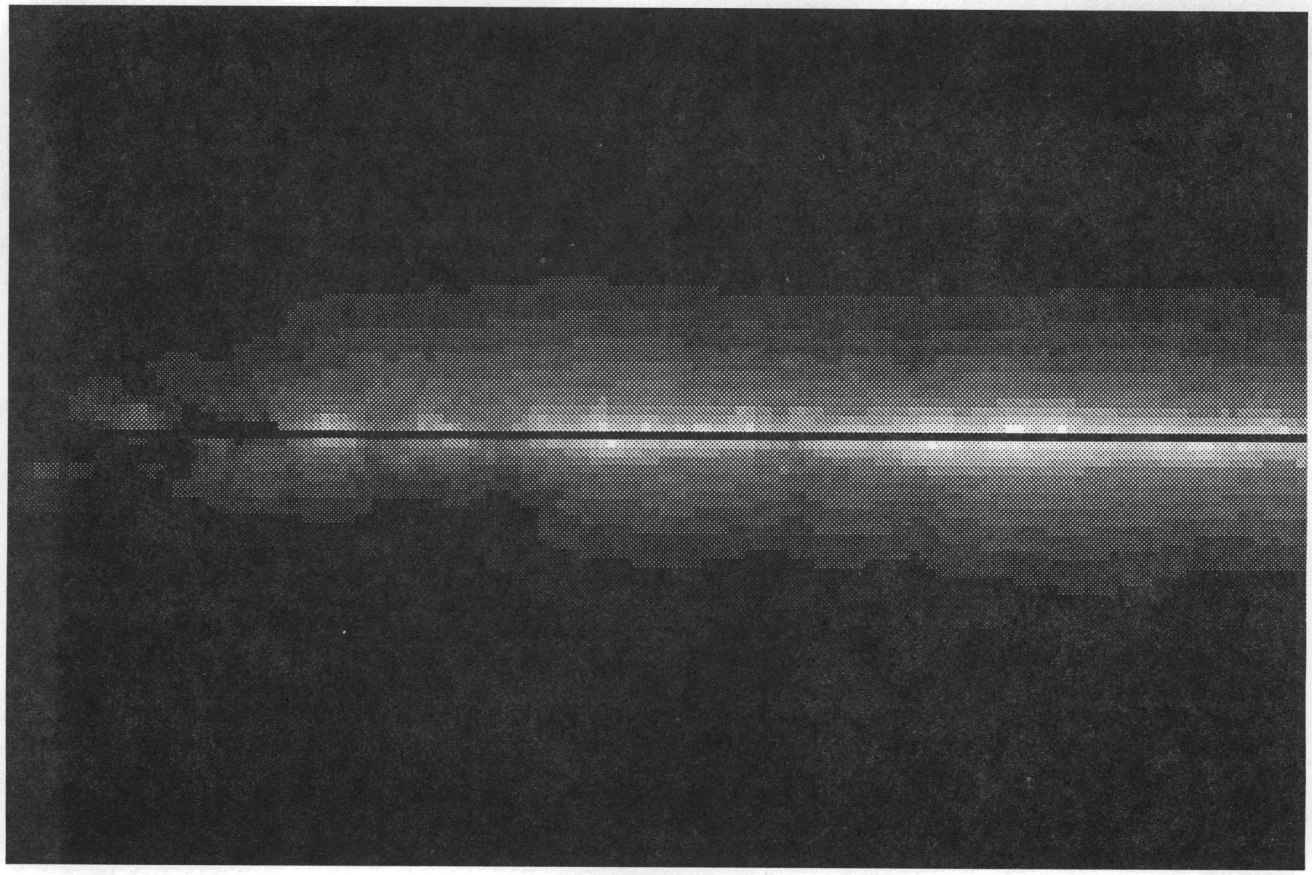

FIG. 13*b*

FIG. 13.—(*a*) A face-on view from the north Galactic pole of our standard cloud model in emission measure (corrected for cloud brightness) centered on the Sun's location encompassing a 10 kpc square region at 50 pc resolution. (Recall the catalog incompleteness beyond 2.5 kpc from the Sun.) (*b*) An edge-on view from $l = 270°$ of our standard cloud model in emission measure (corrected for cloud brightness) centered on the Sun's location extending 10 kpc in the plane and 5 kpc thick at 50 pc resolution. (*c*) Same as 13*b*, but including interstellar extinction.

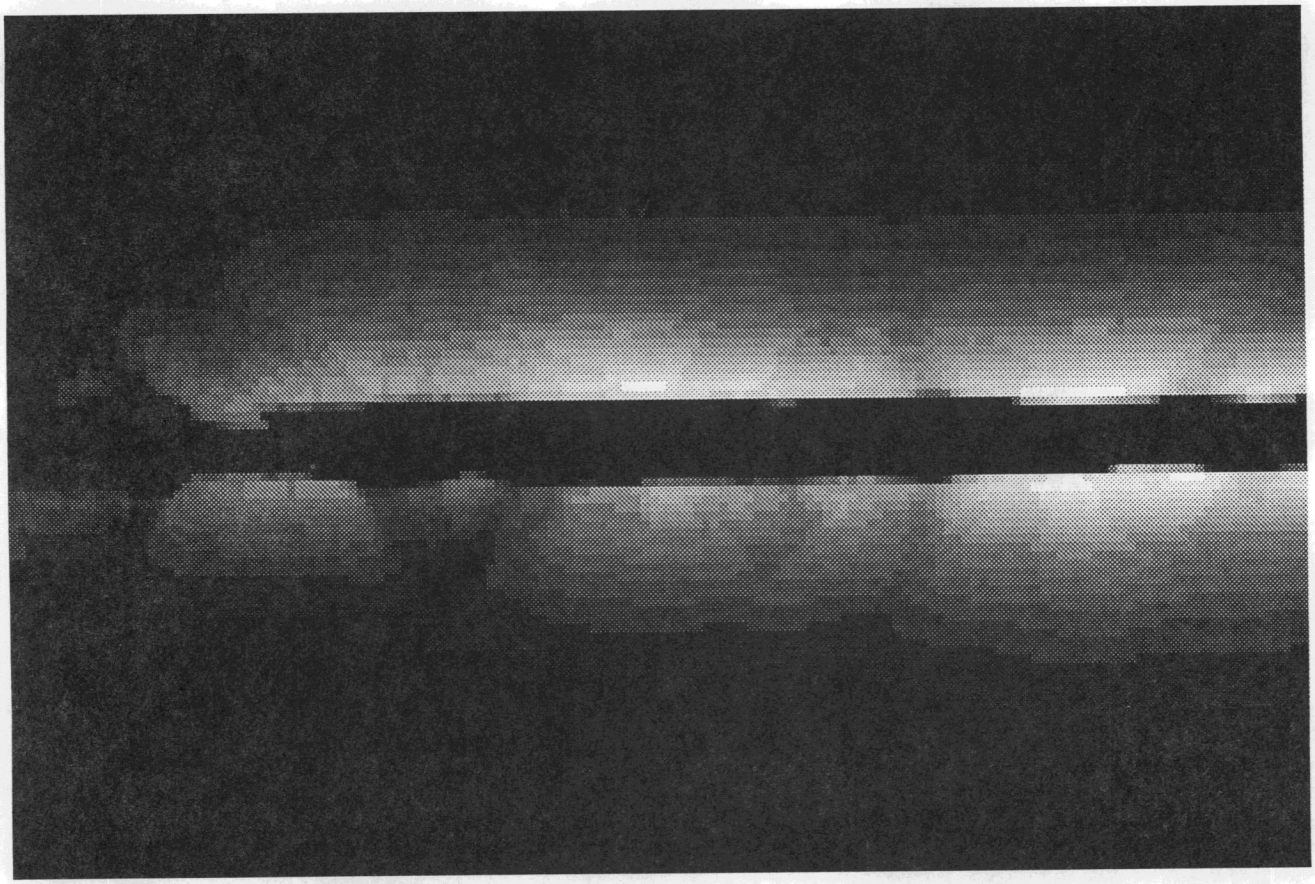

FIG. 13c

for a 2.5 kpc radius), yet the $\pm z$ asymmetry persists even at these large scales. Caution is thus in order when comparing low-latitude kiloparsec-length sight lines with sight lines near the Galactic poles (that sample only very local gas) as is done, for example, when estimating the scale height of the H II layer.

The midplane mean electron density remains fairly constant at ~ 0.06 cm^{-3} in the three volumes and is considerably smaller than in the cloud-free model. However, it is about a factor of 2 larger than the electron density normally attributed to the DISM at the midplane. Recall also that we found only a modest variation of $\langle n_e \rangle_0$ with different choices of the cloud mean free path and the midplane extracloud hydrogen density (those model parameters expected to affect $\langle n_e \rangle_0$ the most) in § 4.2.2. The computed mean square electron density (excluding the cloud boundary contribution) at the midplane (Fig. 8), about 0.008 cm^{-6}, together with $\langle n_e \rangle_0 = 0.06$ cm^{-3} imply a

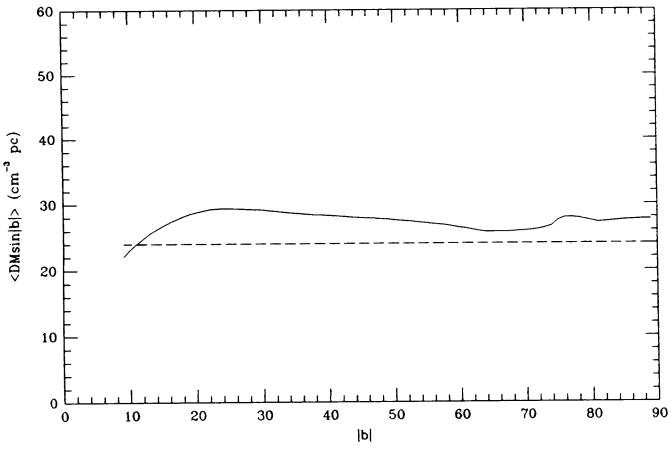

FIG. 14.—The component of the dispersion measure perpendicular to the Galactic plane averaged over Galactic longitude vs. $|b|$ for $|b| > 10°$, for the standard cloud model (*solid curve*). The dashed line is the average observed dispersion measure.

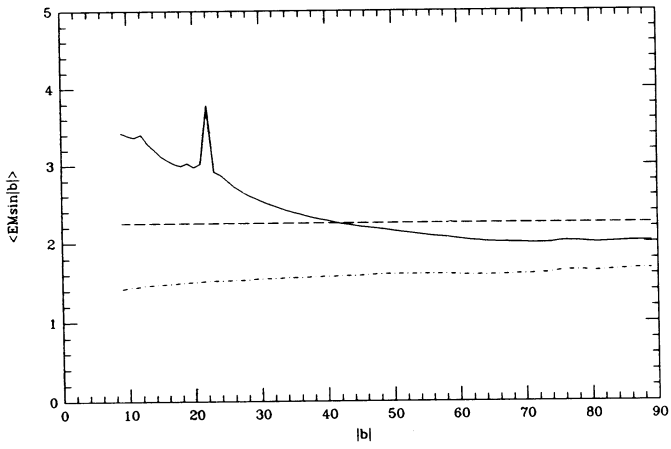

FIG. 15.—The component of the emission measure perpendicular to the Galactic plane averaged over Galactic longitude vs. $|b|$ for $|b| > 10°$, for the standard cloud model (*solid curve*). The dashed line is the average observed emission measure. The large spike in the solid curve at $b = 23°$ is due to a nearby O star (ζ Oph). The dot-dashed curve is the emission from the extracloud medium alone.

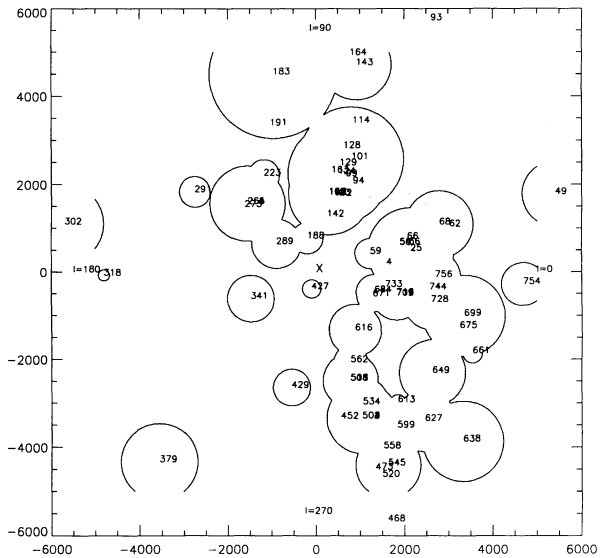

FIG. 16*a*

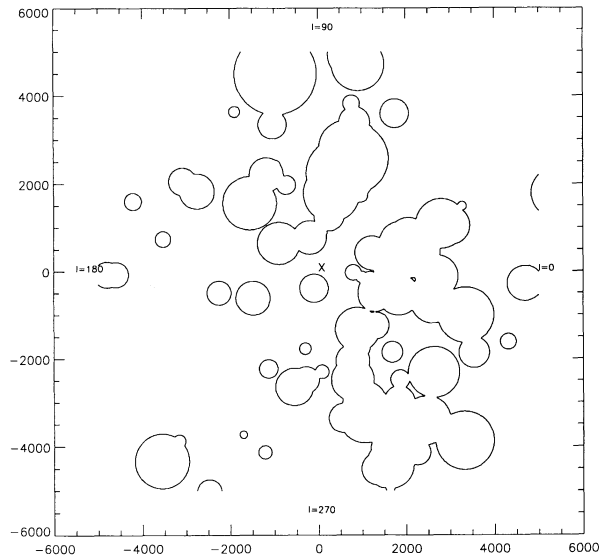

FIG. 16*b*

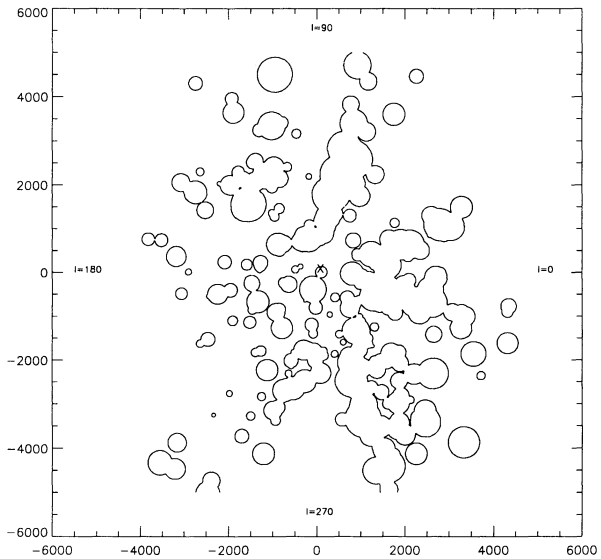

FIG. 16*c*

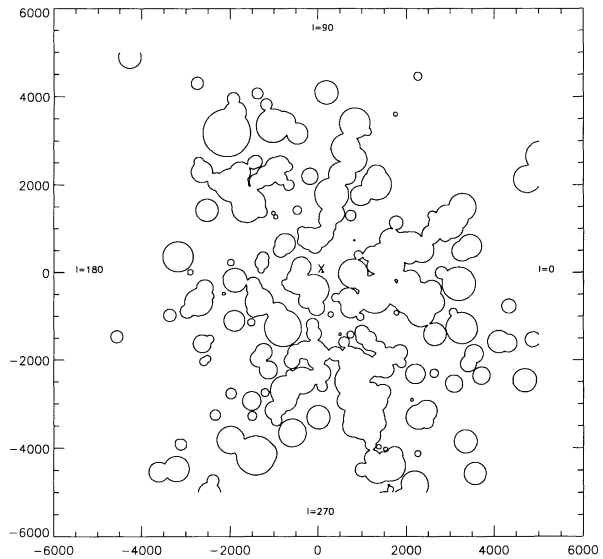

FIG. 16*d*

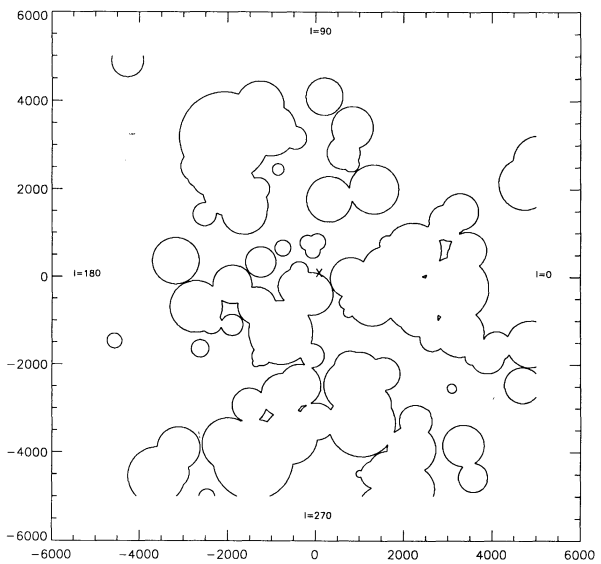

FIG. 16*e*

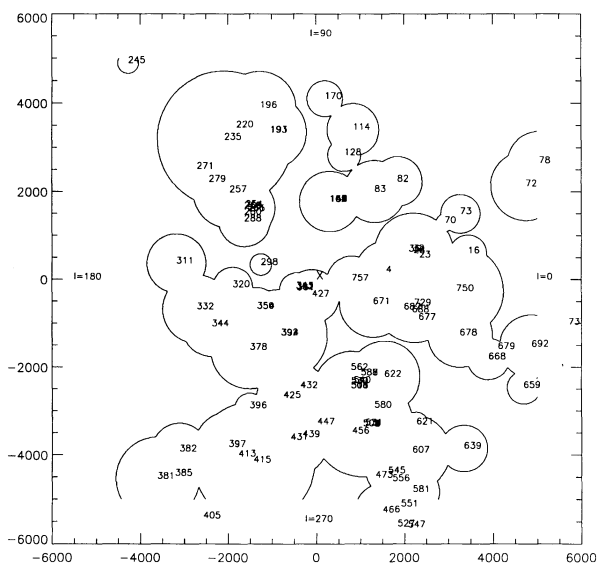

FIG. 16*f*

FIG. 16.—(*a*) A horizontal slice through the standard cloud model at $z = +800$ pc illustrating the H II regions at this height above the plane. The Sun's location is marked by a cross at the center, the longitudinal directions are indicated at the edge of the plot, and the scale is parsecs. The stars responsible for the ionization in the slice are numbered and indexed in Table 2. (*b*) Same as in *a*, but at $z = +400$ pc (star names not indicated). (*c*) Same as in *a*, but at $z = +100$ pc (star names not indicated). (*d*) Same as in *a*, but at $z = -100$ pc (star names not indicated). (*e*) Same as in *a*, but at $z = -400$ pc (star names not indicated). (*f*) Same as in *a*, but at $z = -800$ pc (star names indexed in Table 3).

TABLE 3

INDEX TO STARS IN FIGURE 16*f*

Index	Star Name	Index	Star Name	Index	Star Name
0	HD 164019	279	HD 15137	504	HD 93129B
3	HD 168941	280	HD 16691	506	CPD −582620
4	HD 164794	288	HD 14633	508	CPD −592603
16	HD 210809	298	HD 41161	511	CPD −592600
23	HD 167659	311	HD 242908	513	HD 93027
28	HD 175876	320	HD 36879	527	HD 305560
32	HD 175754	332	HD 39680	530	HD 303558
36	HD 168076	343	HD 36486	531	HD 93843
70	HD 173010	344	HD 36841	540	HD 96042
72	HD 173783	350	HD 46150	545	HD 96670
73	HD 172175	352	HD 37742	547	CPD −612030
77	HD 173820	354	HD 46223	550	HD 96264
78	BD −054769	361	HD 37043	551	MART 121
82	HD 198864	371	S2891	556	HD 96355
83	HD 188001	378	HD 36619	559	HD 97848
114	HD 228766	381	LSS 207	560	MART 156
128	HD 229232	382	S3011	562	HD 95992
148	BD +404220	385	S3061	580	HD 100099
150	CYGOB 222	392	HD 38666	581	HD 99856
151	CYGOB 29	393	HD 57060	585	HD 101223
152	BD +404227	394	NGC 236264	587	HD 101191
154	CYGOB 28C	396	HD 63005	588	HD 101190
155	CYGOB 28B	397	HD 60369	607	HD 106871
157	CYGOB 27	405	CD −265285	621	CD −613452
159	CYGOB 23	409	HD 66788	622	HD 113606
162	BD +413807	413	CD −295191	639	HD 120521
170	HD 202124	415	HD 61827	659	HD 127493
185	HILTNER 241	425	HD 68450	668	HD 146628
191	HD 215835	427	CPD −352212	671	HD 148937
193	BD +552840	431	HD 73882	674	HD 149452
196	HD 218915	432	HD 69648	677	HD 328209
220	HD 1337	439	CD −444865	678	HD 328856
235	HD 5005A	447	CD −484352	679	HD 150958
245	BD +59367	456	HD 302501	687	CD −4511034
254	HD 13268	459	HD 90273	688	CD −4511051
257	BD +62424	460	HD 88412	692	HD 151003
261	HD 15558	466	HD 91824	729	HD 155873
265	HD 15570	469	HD 92850	737	HD 155775
268	HD 14947	473	HD 91651	750	HD 155806
269	HD 14434	502	HD 93249	757	HD 161789
271	HD 15642	503	HD 93128		

midplane H II filling factor of 45%, again nearly a factor of 2 too large.

The statement that our model $\langle n_e \rangle_0$ exceeds that in the DISM, however, is based solely on simple electron density models fit to the pulsar dispersion measure data. Just how reliably these models represent the electron density in the DISM is to us still questionable. Observationally, the mean midplane electron density is inferred from dispersion measures to low-latitude pulsars at a known distance d, sampled over a large volume of the Galaxy; one then has $n_e = \mathrm{DM}/d$ for many sight lines from which an estimate of $\langle n_e \rangle_0$ can be made. Of course, the average is over a slab of gas with a thickness representative of the pulsar z distribution in the sample, not just at $z = 0$, which will give a number lower than the actual $\langle n_e \rangle_0$ simply because of the exponential fall off of $n_e(z)$. For example, one sample of low-latitude pulsars used to determine $\langle n_e \rangle_0$ had an average pulsar z of 115 pc (Vivekanand & Narayan 1982), a volume of space over which our model electron density changes by 25%.

Many authors attempt to separate the contribution to the electron density from sources other than the ionized DISM, most often that from "traditional" H II regions and, more recently, the Galactocentric radial dependence of n_e (Vivekanand & Narayan 1982; Cordes et al. 1991) when creating an electron density model. Without the traditional H II region contribution, typical models that are consistent with the pulsar dispersion measures have a midplane mean density of 0.025 cm^{-3}, although there is some scatter about this value among the various models (Hall 1980 claims $\langle n_e \rangle_0$ is as large as 0.048 cm^{-3}).

A potential problem with this reduced estimate of $\langle n_e \rangle_0$ is the assumption that traditional H II regions contribute substantially to n_e along every sight line. The number usually quoted as the traditional H II region contribution to n_e at the midplane (0.015 cm^{-3}) is derived analytically from a highly oversimplified statistical average of the population of nearby hot stars and the Strömgren spheres they would produce in a uniform, high-density medium (Prentice & ter Haar 1969; Lyne et al. 1985). In fact, the filling factor of what should be termed "traditional" H II regions (the relatively few bright, nebulous H II regions we are accustomed to seeing in the Palomar Sky Survey prints and, mistakenly, associate with all H II regions) is very small given the typical Strömgren radius of an O star in a high-density medium ($R_s \leq 50$ pc for $n \geq 1.0$ cm^{-3}). Thus, it is improbable that a pulsar sight line intercepts the densest portion of any H II region (with the exception of

sight lines through nearby regions like the Gun nebula that cover a substantial portion of the sky). Furthermore, if O stars ionize the DISM they do so *inside* their H II regions which are properly thought of as large, diffuse volumes of ionized gas. It is the aggregate of these H II regions that we think of as the ionized part of the DISM. A mean midplane electron density of 0.025 cm^{-3} might be more representative of the *lowest* column density sight lines through the DISM that happen not to intercept denser condensates (diffuse clouds maybe). Issues of this sort should be resolved as more detailed observations of the DISM continue.

An alternative method of examining the pulsar dispersion measure data that is both informative and independent of the exact midplane value of the electron density in the DISM is to plot the vertical component of the electron column density in the direction to pulsars at a known distance against z as Reynolds (1989b) has done (reproduced here in Fig. 10). Figure 9 contains our standard cloud model version of this plot. Overlaid on both figures is a typical model taken from the literature (*dashed line*) of the total electron density (DISM plus traditional H II regions) as a function of z. The electron density model fits the data in both figures reasonably well given the uncertainties. Also evident in the figures is the extent of the electron layer to high z as well as the common slope at low to moderate z (which is an indication of constancy of the electron density near the midplane in the linear approximation to the exponential fall off of n_e). Our model results appear to be offset vertically in Figure 9 by a constant amount (in the log) corresponding to roughly a factor of 1.5 in the mean density, but it is difficult to tell with the small number of data points.

A further test of our model is how well it matches the dispersion measure along the individual sight lines appearing in Figures 9 and 10. In Figure 11, note that our model agrees with all but a few of the pulsar measurements to within better than a factor of 2. The overestimation of the low-latitude sight lines in Figure 11 is indicative of the large H II filling factor near the midplane of our model as discussed earlier. One of the less well fitted sight lines (marked as a cross) is that to PSR 0823+26 which has been independently studied in great detail.

Reynolds (1990b, 1992) examined the known sources of ionization along the path to the pulsar PSR 0823+26. It has a well-determined distance via VLBI parallax (Gwinn et al. 1986) of 360 ± 80 pc, and a dispersion measure of 19.46 cm^{-3} pc. Reynolds (1990b) notes that none of the B stars or hot white dwarfs in the region sampled by this sight line come within a factor of 10 of being able to produce this column of electrons. The only remaining candidates are three O stars, each of which must be able to ionize long paths through the Galactic disk. Our standard cloud model underestimates the dispersion measure in the direction of PSR 0823+16 for a line segment length of 360 pc (accumulating only 3.94 cm^{-3} pc). However, the cloud-free model has a dispersion measure along the same sight line that well exceeds (33.71 cm^{-3} pc) the measured quantity. It is not inconceivable then that O stars are responsible for the electron column toward PSR 0823+16 given the availability of ionizing photons as suggested by the cloud-free model. Apparently, what does matter in this direction is the distribution of absorbing clouds; in particular, it must do better than our cloud model of allowing photons from the candidate O stars to ionize regions along this sight line.

Much of the comparison between pulsar dispersion measures and sight lines through our model can be summarized by the dependence of $\langle \mathrm{DM} \sin |b| \rangle$ on Galactic latitude in Figure 14. Whereas $\langle \mathrm{DM} \sin |b| \rangle$ substantially exceeds the observational average in the cloud-free model (Fig. 5), the agreement is much better in the standard cloud model.

An issue of great concern is whether O star H II regions can match the observed Galactic Hα background as well. Cox (1989) has shown that supernova remnants could potentially produce enough diffuse electrons to explain the pulsar dispersion measures, but would fall short of providing the Hα brightness by a factor of 7. Besides there being a well-measured average cosecant dependence on latitude of the Hα emission at latitudes greater than 15°, there is a marked reduction in intensity near the Galactic poles. Models attempting to explain the Hα background must get both of these features correct (one characteristic of a large volume of space, the other a local phenomena above the Sun). In our standard cloud model, although the clouds have greatly diminished the emission measure from the photoionized extracloud medium in the plane (Fig. 15, *dot-dashed curve*), the combined emission including that from ionized cloud surfaces (*solid curve*) easily accounts for the high brightness seen at low latitudes. (The emission measures in Fig. 15 are not corrected for interstellar reddening.) Moreover, the lower than average brightness at high latitudes is reproduced by our model.

Several complications we neglect in our model could alter the filling factor of H II near the plane of the Galaxy. The ability of stellar photons to reach distant places depends strongly on conditions close to the stars. For our model, nothing is special about these locations, but in reality such locations tend to be atypical. The stars are located near molecular and atomic gas concentrations, in regions where photoevaporation of clouds is active, and in clusters that tend to create wind- and supernova-blown cavities. It should also be mentioned that additional sources of H II surely exist, particularly in the plane, that complicate the situation at low z. Of these, the Strömgren volumes of early B stars (smaller than O Strömgren volumes, but more numerous) and supernova remnants are probable contributors to $\bar{n}_e$. We discuss briefly below some of these localized phenomena and their impact on our results.

Some O stars are near the large molecular cloud complexes from which they formed and, hence, have a significant fraction of their radiation solid angle covered by clouds. It is uncertain how many stars fall into this category, but the numbers should be greatest near the midplane (especially in spiral arms) where there is an observed concentration of large molecular clouds. To this end, we investigated a highly restrictive, idealized model in which the stars had an asymmetric luminosity chosen to approximate a blister model (an O star embedded in the edge of a molecular cloud) geometrically. For a circular radiation pattern with the star on the cloud edge, $\frac{3}{4}$ of the ionizing photon flux is absorbed locally allowing only one-fourth of the photons to escape the vicinity of the blister. Since most stars are not covered by large clouds, this approximation, when applied to all of the stars in the solar neighborhood, serves only as an upper limit to molecular cloud absorption of ionizing photons. But it does suggest that in an environment like the midplane where the distributions of molecular clouds and O stars overlap, the average solid angle available for O stars to radiate into could be reduced by factors of a few (preferentially planar radiation), resulting in a similar decrease of the H II filling factor there.

Elmegreen (1976) investigated the photoevaporation of a uniform distribution of identical H I clouds by O stars over

their lifetime in an otherwise low-density interstellar medium. He concluded that the mean effective density in the immediate surroundings of an O star eventually increases to unit density, thereby significantly reducing the size of the Strömgren volume. More recently, McKee, Van Buren, & Lazareff (1984) have expanded on this work by including a distribution of cloud masses and stellar wind–blown bubbles, at a basic level concurring with Elmegreen's (1976) conclusions. Considering only the photoevaporation of clouds, McKee et al. (1984) found that the radius of the region homogenized by an O star is independent of spectral type, depending only on the mean density surrounding the star. This result allows us to relate our statistical clouds is a simple way to the reduced Strömgren volume due to the photoevaporation of clouds. Drawing from the results of McKee et al. (1984), we have found that for an O6 zero-age main-sequence star the depletion of stellar flux by balancing recombination within a homogenized cloud zone of unit density is comparable to that from encounters with the statistical clouds close to the star in our model. For stars earlier than O6, our clouds attenuate somewhat more, while for later types they do less. As a result, our model is conservative (at least for early O stars) in accounting for the reduced Strömgren volume associated with photoevaporation of clouds. Combination environments have not been thoroughly studied theoretically, with long-lived bubbles and continued photoevaporation from multiple stars of different lifetimes, but the best hope of discovering the net effect will come from observational work on ionizing photon leakage from cloudy H II regions.

Cavities produced by supernova explosions or stellar winds of early-type stars either singly or, in the case of superbubbles, by many stars, will tend to decrease the photon losses near the stars. However, the issue is more complex since a cavity presumably has a dense surrounding shell that will increase the losses there. Which effect dominates depends strongly on the shell irregularities and scale and can probably best be determined, once again, from observational studies of photon leakage.

In the introduction we pointed out two characteristics required of the interstellar medium if O stars are to provide the diffuse ionization: the ionizing photons must have long mean free paths between encounters with clouds, yet there must be a sufficient density of intercloud material to provide the required fluorescence to Hα. A careful reader may have noticed that we have not proved that either of these characteristics is present in the true interstellar medium. We built both into our model, however: by choosing an absorption mean free path at the midplane of 160 pc and an absorber scale height of only 100 pc, we guarantee that there are many clear sight lines to high latitude. Similarly, by including an intercloud component whose midplane density is similar to the local density inferred for ionized gas in the plane, and whose density at high z is just that inferred from the ionized gas parameters, it would seem that we could not have failed to get results which resembled the Galaxy.

Reynolds (1990a) has estimated that roughly 15% of the O star ionizing flux would have to escape the neighborhoods of the stars to generate the diffuse ionization. Unless there are solid walls of dense hydrogen surrounding most of the stars, it is difficult to imagine how such escape from near the stars could fail. For the photons to reach high z, however, there need to be open lines of sight to high z. That is, the probability of missing all clouds must exceed 0.15. In the remainder of this section we discuss more thoroughly whether that is a reasonable expectation.

The transparency of the interstellar medium to Lyman-continuum photons is not well known. One is likely to suppose that the photon mean free path is small, because looking outward from the Sun, there are many optical depths of hydrogen in all directions. Much of that hydrogen, however, is seen only in emission implying that it is rather hot and is probably at a low density. A bright O star at the solar location could ionize all low density gas, considerably altering our view of the H I sky. The important opacity thus resides in denser gas, capable of recombining at the rate it is ionized and confining its ionization to cloud surfaces.

The most sensitive studies of denser gas appear to have been made via 21 cm absorption, with the results quoted as $P(\tau)$, the expected number of absorption features with optical depth $\geq \tau$, on a line of sight directed perpendicularly outward from the Galactic plane. Payne, Salpeter, & Terzian (1983, hereafter PST) using Arecibo data found $P(0.062) = 0.72$ while closer to their sensitivity limit, $P(0.015) \approx 1.35$. The number of features found continues to increase with decreasing τ, down to the sensitivity limit of the telescope. As a result, the $P(0)$ is not known. One clue, however, is that on average, decreasing τ is accompanied by increasing temperature. In addition, the data (e.g., Fig. 5 of PST) appear to be bounded on the top by an upper limit temperature of 300 K. Kulkarni & Heiles (1987) noted that there are good reasons for expecting such a limit. Cox (1988) showed that both upper and lower bounds on cloud temperatures (with the range exhibited by the T-τ relation) should be present in a medium with significant magnetic pressure. By examining the distribution of features on a T-τ diagram (the figure referred to above), we have concluded that $P(\tau)$ should have an asymptote as $\tau \rightarrow 0$ no greater than about 2.5, though one cannot be certain that the trends from larger τ can be extrapolated.

In order to convert $P(\tau)$ to a vertical distribution of photon mean free paths, we need the vertical distributions of each τ. Given the imprecision with which $P(\tau)$ is known, we take as sufficient knowledge the mean height information quoted in Kulkarni & Heiles (1987): 88 pc for $\tau > 0.1$ and 229 pc for $\tau < 0.1$. Then, assuming the higher and lower τ clouds have Gaussian and exponential distributions, respectively, we infer

$$\frac{1}{\lambda(z)} = \frac{P(0.1)}{88 \text{ pc}} \sqrt{\frac{2}{\pi}}\, e^{-1/2(z/88 \text{ pc})^2} + \frac{P(0) - P(0.1)}{229 \text{ pc}}\, e^{-(z/229 \text{ pc})} . \quad (17)$$

From the previous discussion, we expect $P(0)$ in the range 1.3–2.5 (the lower value being the observed value at the telescope sensitivity limit), while PST suggest $P(0.1) \approx 0.75$.

There are several other factors, however, which make it difficult to believe that these results can be considered reliable for our purposes. The Arecibo results derive from emission-absorption studies on a rather small number of sources (~ 30) distributed over the sky. A much larger survey of several hundred sources in the Nançay catalog (Crovisier 1981) obtained somewhat different results and found that $P(\tau)$ depended on the latitude of the sources used to derive it. For $|b| > 30°$, he found $P(0.062) \approx 0.5$ (vs. 0.72 from PST's data table and 0.91 from their functional approximation). For $5° < |b| < 30°$, Crovisier obtained $P(0.062) = 0.25$. It has been suspected that these differences derive from line blending on

long sight lines, making it more difficult to separate an absorption spectrum into the correct number of features. This explanation may apply to the difference between the results at high and low latitude from the Nançay data, but it cannot possibly be a correct interpretation of the difference between the Nançay and Arecibo results, because a significant fraction of the Nançay spectra showed no absorption at all to the limiting sensitivity. Weak features were not missed in blends if there were no blends.

There may be other observational factors contributing to this discrepancy, but there is almost certainly an important astrophysical reason as well: if individual clouds have internal velocity structures, or equivalently there are clusters of clouds, then the number of velocity features on a sight line is not a good measure of the probability of encountering clouds. One must divide by the mean number of features per encounter. Even if that number is only 1.5, it has a large impact on the Lyman-continuum opacity.

There are two other potentially important complications, both arising from the data's having been taken from the solar location. The Sun is in a particular environment, inside a low-density bubble thought to contain 10^6 K gas. If the formation of that bubble has distorted the cold H I distribution in our vicinity, for example by pushing it into a shell or shredding it into cirrus, then the view from here may not be representative. A study by Garwood & Dickey (1989) has examined sources in the Galactic plane and differentiated over the rotation curve. They find noticeably fewer absorptions per kiloparsec in the inner Galaxy, but the results closer to the solar circle are comparable to the high latitude ones. The solar location is not different by a large factor, but even a modest factor could be critical.

The second of these complications is that we cannot tell whether the H I features at low τ are equally likely to be found in both neutral and ionized parts of the DISM. If they are in some way formed as transients in the H I zones, perhaps in response to the overpressure in neighboring ionized regions, then they will not be present on the ionizing photon paths.

As we have mentioned, the opacity of the DISM to Lyman-continuum photons from O stars is not well known. Intercomparison between the various H I studies leads us to expect that the PST results and our extrapolation to $\tau = 0$ underestimate the intercloud mean free path by a factor 1.5–2. As a consequence, we adopt $P(0.1) = 0.5$ and $P(0) = 1.5$ as plausible values for use with equation (17) for a test of whether the low-τ clouds have a major impact on our results on the ability of the O stars to maintain the widespread ionization of the DISM. The corresponding mean free path at $z = 0$ is 112 pc, with each component (thin and thick) being equally important. The flux attenuation factor from the midplane to infinity at high latitude is $e^{-P(0)} = 0.223$. For comparison, our standard cloud model has a mean free path of 160 pc and a vertical attenuation of 0.46 [$P(0) = \tau = 0.783$].

Using $P(0.1) = 0.5$ and $P(0) = 1.5$ with equation (17), we computed the Strömgren volumes and the various measures discussed earlier in regard to the standard cloud model. As might be expected, a thicker distribution of clouds with a shorter mean free path between encounters reduces the flux of ionizing photons to high z. Furthermore, larger numbers of photons are captured on cloud surfaces relative to those that ionize the DISM than in the standard cloud model. This has the effect of both increasing the contribution to the Hα background from cloud surfaces at low latitudes and diminishing the emission from the diffuse gas at all latitudes due to the loss of photons on cloud surfaces at low z and the paucity of ionizing photons reaching high z. The result is the total $\langle \mathrm{EM} \sin |b| \rangle$ at high latitudes is smaller by 30% relative to the standard case (Fig. 15). The shorter mean free path at the midplane reduces the mean electron density there by $\leq 15\%$ over the standard case, bringing it closer to the observed value. Similarly, the dispersion measures to the pulsars in Figures 9 and 10 are slightly smaller, in general, producing a better match to the observational electron density model in the figures (*dashed line*). The comparison of individual pulsar dispersion measures with sight lines in the model (as in Fig. 11) is also better, although certain sight lines remain poorly fitted.

Overall, this cloud description still allows extensive O star photoionization of the DISM, albeit more confined to the Galactic plane, and does not grossly change the character of the standard cloud model results. The uncertainty in the numbers and distribution of low column density clouds in the Galaxy and how appropriate an extrapolation is from higher column density cloud measurements precludes a more detailed study using our model. However, it should be mentioned that in many ways our models are conservative in regard to producing ionization in the DISM. Uncertainty in the luminosities of the stars was not considered, but is clearly an important parameter. The difficult issue of Strömgren volume overlap and the extra photons it supplies is likely an important effect that we cannot model. This is because of the clumpiness of the O star distribution in the Galaxy, and the fact that a decreasing hydrogen density with z results in an increasing H II region diameter as the distance from the midplane grows. If overlap is common among O star H II regions above the layer populated by clouds, additional ionizing photons will escape to high z beyond the union of isolated H II regions as computed in our models. We have computed the component of the total ionizing photon flux perpendicular to the disk at various z distances from the midplane in the 2.5 kpc completeness region around the Sun, and compared it to the total flux of ionizing photons available from O stars in a similar sized region as given by Abbott (1982). The results, summed over both sides of the Galactic disk, for $|z| = 200$, 500, and 1000 pc are 19%, 8%, and 4%, respectively. The neglect of H II region overlap clearly makes these ratios lower limits, but they are in the neighborhood of the fraction required to account for Hα recombinations observed at high latitudes by Reynolds (1990a), who estimates roughly 15% of the O star ionizing flux must escape to high z.

6. CONSEQUENCES

If O stars provide the bulk of the ionization in the diffuse interstellar medium, including that far off the plane, then there are some rather firmly predictable consequences which should resemble features of our model.

1. A significant fraction of the diffuse Hα background arises on cloud surfaces rather than from intercloud gas, particularly at low latitudes and when low column density clouds are present in large numbers. This is much less true of the dispersion measures, however, if all cold H I is dense. This difference affects one's estimate of the ionized gas filling factor and local densities. For example, Reynolds (1991) estimates the high-latitude mean filling factor to be $f \geq 0.2$ and the local $\bar{n}_e = 0.08$ cm^{-3}. If only $\frac{2}{3}$ of the Hα is truly diffuse, the gas is less clumped by that fraction ($f \geq 0.3$) and correspondingly less dense ($\overline{n_e} \approx$

0.06 cm^{-3}). In addition, the cloud boundary emission drops off much more rapidly with z than does that of the diffuse component.

2. The diffuse Hα emissivity and electron distribution should exist primarily around and above the concentrations of O stars. We illustrate this point with six horizontal slices through our calculated H II regions (Fig. 16) at $z = \pm 100$ pc, $z = \pm 400$ pc, and $z = \pm 800$ pc. For the $z = \pm 800$ pc slices, the brightest stars contributing to the predicted ionization locations are indicated.

3. Velocity information in the Hα spectra should make it possible to explore the relationship between O stars and ionized gas. For example, we have rerun our standard cloud model, restricting the catalog only to those stars thought to be within the Perseus arm, an easily distinguishable feature in the Hα spectra. It is clear from the emission measure map that this arm should have a patchy distribution of Hα that is closely associated with the stellar locations.

4. Face-on views of galaxies such as ours are likely to show faint diffuse Hα nearly everywhere due to a superposition of features as well as nearly full ionization at great z. At high intensity one sees only the ionization of dense gas close to the stars while at intermediate intensity, the very large diffuse H II regions of the brightest stars appear to fill much of the surface, similar to the "froth" found in M33 by Courtès et al. (1987).

5. The vertical structure of the Hα surface brightness of a galaxy such as ours seen edge-on should be intrinsically very bright near the plane due to the cloud surfaces and fall off rapidly with little projected structure. On the other hand, when extinction is included, one's view is much more constrained. The plane becomes dark, possibly with a bright rim, and the higher z surface brightness becomes much more structured as our view is restricted to the nearer portions (see Fig. 13).

7. CONCLUSIONS

Using all known O stars in the solar neighborhood, a smooth estimate of the extracloud neutral hydrogen density as a function of z in the diffuse interstellar medium, and a statistical approximation of H I clouds, we have calculated the H II region structures and have shown that they produce ionized gas properties that are consistent with the observations of the diffuse ionized gas in the Galaxy. Even with the simplified assumptions of our standard cloud model, good quantitative agreement is found for the electron density as a function of z and the dispersion measures to pulsars at high and low latitudes as well as quantitative agreement for summary measures such as the mean vertical column density of electrons, the average Hα surface brightness perpendicular to the galactic plane, and its decrease at high latitude. We probably found too large a mean midplane electron density, but this is not surprising given the shielding expected from clouds near the stars. When low column density clouds were considered, much more of the ionizing photon flux was captured on cloud surfaces resulting in lower extracloud electron densities and a larger fraction of the Hα emission arising from cloud surface recombination. Our model suggests that the ionized part of the diffuse interstellar medium consists of the dilute portions of O star H II regions, as was suspected from the power necessary to sustain the ionization, the temperature of the ionized gas, and the emission spectrum.

We would like to acknowledge many useful discussions with Ron Reynolds. We also thank the Astronomical Data Center at the NASA/Goddard Space Flight Center for providing the O star catalog in machine readable form. This research was supported by the National Aeronautics and Space Administration under grants NAWG-2532 and NAG 5-629.

REFERENCES

Abbott, D. C. 1982, ApJ, 263, 723
Bregman, J. N., & Harrington, J. P. 1986, ApJ, 309, 833
Cordes, J. M., Weisberg, J. M., Frail, D. A., Spangler, S. R., & Ryan, M. 1991, Nature, 354, 121
Crovisier, J. 1981, A&A, 94, 162
Courtès, G., Petit, H., Sivan, J.-P., Dodonov, S., & Petit, M. 1987, A&A, 174, 28
Cox, D. P. 1988, in Supernova Remnants and the Interstellar Medium, ed. R. Roger & T. Landecker (New York: Cambridge Univ. Press), 73
———. 1989, in IAU Colloq. 120, Structure and Dynamics of the Interstellar Medium, ed. G. Tenorio-Tagle, M. Moles, & J. Melnick (New York: Springer Verlag), 500
———. 1990, in IAU Symp. 147, Fragmentation of Molecular Clouds and Star Formation, ed. E. Falgarone (Dordrecht: Kluwer), 3
Dettmar, R.-J. 1990, A&A, 232, L15
Dettmar, R.-J., & Schulz, H. 1992, A&A, 254, L25
Elmegreen, B. G. 1976, ApJ, 205, 405
Garmany, C. D., Conti, P. S., & Chiosi, C. 1982, ApJ, 263, 777
Garwood, R. W., & Dickey, J. M. 1989, ApJ, 338, 841
Gwinn, C. R., Taylor, J. H., Weisberg, J. M., & Rawley, L. A. 1986, AJ, 91, 338
Hall, A. N. 1980, MNRAS, 191, 751
Harding, D. S., & Harding, A. K. 1982, ApJ, 257, 603
Kulkarni, S. R., & Heiles, C. 1987, in Interstellar Processes, ed. D. Hollenbach & H. Thronson (Dordrecht: Reidel), 87
Kurucz, R. L. 1979, ApJS, 40, 1
Lynds, B. T. 1980, AJ, 85, 1046
Lyne, A. G. 1981, in IAU Symp. 95, Pulsars, ed. W. Sieber & R. Wielebinski (Dordrecht: Reidel), 423
Lyne, A. G., Manchester, R. N., & Taylor, J. H. 1985, MNRAS, 213, 613
McKee, C. F., Van Buren, D., & Lazareff, B. 1984, ApJ, 278, L115
Manchester, R. N., & Taylor, J. H. 1981, AJ, 86, 1953
Mathis, J. S. 1986, ApJ, 301, 423
Panagia, N. 1973, AJ, 78, 929
Payne, H. E., Salpeter, E. E., & Terzian, Y. 1983, ApJ, 272, 540 (PST)
Prentice, A. J. R., & ter Haar, D. 1969, MNRAS, 146, 423
Rand, R. J., Kulkarni, S. R., & Hester, J. J. 1990, ApJ, 352, L1
———. 1992, ApJ, 396, 97
Reynolds, R. J. 1984, ApJ, 282, 191
———. 1985, ApJ, 294, 256
———. 1989a, ApJ, 345, 811
———. 1989b, ApJ, 339, L29
———. 1990a, in IAU Symp. 144, The Interstellar Disk/Halo Connection in Galaxies, ed. H. Bloeman (Dordrecht: Kluwer), 67
———. 1990b, ApJ, 348, 153
———. 1991, ApJ, 372, L17
———. 1992, in Massive Stars: Their Lives in the Interstellar Medium, ed. J. Cassinelli & E. Churchwell, in press
Reynolds, R. J., & Cox, D. P. 1992, ApJ, 400, L33
Sokolowski, J., & Bland-Hawthorne, J. 1992, preprint
Spitzer, L. 1978, Physical Processes in the Interstellar Medium (New York: Wiley), 156
Thuan, T. X. 1975, ApJ, 198, 307
Torres-Peimbert, S., Lazcano-Araujo, A., & Peimbert, M. 1974, ApJ, 191, 401
Weisberg, J. M., Rankin, J. M., & Boriakoff, V. 1980, A&A, 88, 84
Vivekanand, M., & Narayan, R. 1982, J. Astrophys. Astron., 3, 399